



OPEN

Whole-brain mapping of monosynaptic inputs to midbrain cholinergic neurons

Icnelia Huerta-Ocampo¹, Daniel Dautan^{1,2}, Nadine K. Gut¹, Bakhtawer Khan¹ & Juan Mena-Segovia^{1✉}

The cholinergic midbrain is involved in a wide range of motor and cognitive processes. Cholinergic neurons of the pedunculopontine (PPN) and laterodorsal tegmental nucleus (LDT) send long-ranging axonal projections that target sensorimotor and limbic areas in the thalamus, the dopaminergic midbrain and the striatal complex following a topographical gradient, where they influence a range of functions including attention, reinforcement learning and action-selection. Nevertheless, a comprehensive examination of the afferents to PPN and LDT cholinergic neurons is still lacking, partly due to the neurochemical heterogeneity of this region. Here we characterize the whole-brain input connectome to cholinergic neurons across distinct functional domains (i.e. PPN vs LDT) using conditional transsynaptic retrograde labeling in ChAT::Cre male and female rats. We reveal that input neurons are widely distributed throughout the brain but segregated into specific functional domains. Motor related areas innervate preferentially the PPN, whereas limbic related areas preferentially innervate the LDT. The quantification of input neurons revealed that both PPN and LDT receive similar substantial inputs from the superior colliculus and the output of the basal ganglia (i.e. substantia nigra pars reticulata). Notably, we found that PPN cholinergic neurons receive preferential inputs from basal ganglia structures, whereas LDT cholinergic neurons receive preferential inputs from limbic cortical areas. Our results provide the first characterization of inputs to PPN and LDT cholinergic neurons and highlight critical differences in the connectome among brain cholinergic systems thus supporting their differential roles in behavior.

Acetylcholine is a major neuromodulator that plays a central role in attention, movement and behavioral flexibility. One of the major sources of acetylcholine is located in the midbrain, where cholinergic neurons of the pedunculopontine nucleus (PPN) and laterodorsal tegmental nucleus (LDT) provide widespread innervation to the thalamus^{1–3} and the basal ganglia^{4–8}. Recent studies using genetic approaches to selectively manipulate the activity of cholinergic neurons have shed light into the functions of cholinergic neurons of the PPN and LDT. For example, cholinergic neurons have been shown to be involved in reinforcement learning through the modulation of dopamine neurons in the ventral tegmental area (VTA)⁹ and induce movement through dopamine-mediated mechanisms^{9,10}, particularly in the case of the PPN. In contrast to the classic notions of their involvement in motor activity and wakefulness regulation, however, it has been shown that optogenetic activation of cholinergic neurons in resting mice does not evoke a motor response¹¹, and chemogenetic experiments have shown that activation of cholinergic neurons does not increase the amount of time spent in wakefulness¹². These experiments thus highlight the need to revisit some of the theories of the midbrain cholinergic function. A recent study, for example, has shown that midbrain cholinergic neurons innervate the striatal complex and make direct connections with striatal cholinergic interneurons (CINs); manipulations of either midbrain cholinergic neurons (i.e. PPN/LDT) or CINs have a similar influence on action strategy encoding, suggesting convergent functional roles between midbrain and striatal cholinergic systems¹³. Thus, because the role of acetylcholine across the forebrain has a significant degree of functional overlap (e.g. behavioral flexibility, attention), it is critical to understand how the activity of cholinergic cell groups is regulated by their afferent systems. Recent studies have described the input connectivity of cholinergic neurons of the basal forebrain^{14,15} and the striatum^{16,17} but the sources of inputs to the cholinergic neurons of the PPN and LDT are still missing.

¹Center for Molecular and Behavioral Neuroscience, Rutgers University, Newark, NJ, USA. ²Present address: Department of Neuroscience and Brain Technologies, Genetics of Cognition Laboratory, Istituto Italiano Di Tecnologia, via Morego, 30, 16163 Genova, Italy. ✉email: juan.mena@rutgers.edu

Cholinergic neurons in the PPN and LDT form a continuum that extends from the caudal end of the substantia nigra (SN) to the central gray matter near the fourth ventricle. The efferent connectivity of these two structures is characterized by a topographical arrangement where PPN neurons preferentially innervate motor neuronal systems, whereas LDT neurons preferentially innervate limbic neuronal systems¹⁸. For example, cholinergic neurons of the PPN innervate the dopaminergic neurons of the substantia nigra pars compacta (SNc), the dorsal striatum and thalamic relay nuclei. In contrast, cholinergic neurons of the LDT innervate the ventral striatum and limbic thalamic nuclei. While not entirely segregated, both structures provide converging innervation to a certain subset of structures (i.e. the intralaminar thalamic nuclei, VTA), although detailed examination of the postsynaptic targets at the level of the VTA has revealed a divergent modulation over dopamine efferent circuits⁹, thus suggesting a largely unexplored level of functional selectivity between PPN and LDT cellular targets. Thus, the identification of the afferent systems to PPN and LDT cholinergic neurons is critical to integrate an input/output connectivity map and to understand how their activity is regulated.

Here we aimed to identify and map in whole-brain sections the distribution of presynaptic neurons that specifically synapse onto cholinergic neurons of the PPN and LDT by using a transsynaptic retrograde labeling approach. Our results show a substantial degree of overlap in the structures that innervate both regions but critically reveal a topographical segregation along functionally specialized regions of the cholinergic midbrain that supports previous anatomical and behavioral findings and uncover fundamental differences in the input systems among forebrain cholinergic systems.

Results

Selective targeting of cholinergic neurons in midbrain nuclei. To characterize and map in whole-brain sections the neurons that innervate the cholinergic neurons of the PPN and the LDT, we used a monosynaptic retrograde tracing strategy (Fig. 1A; Callaway and Luo, 2015). For this purpose, we first injected into the PPN and the LDT of male and female ChAT::Cre rats (Fig. 1B) a combination of two helper viruses to induce the conditional (FLEX) expression of a TVA receptor and the rabies glycoprotein (G) in cholinergic neurons. This was followed 2 weeks later by an injection of G-deleted rabies virus in the same locations (SADA-eGFP; Fig. 1A). Neurons expressing the TVA receptor were tagged with mCherry (Fig. 1C, D) and neurons infected with the rabies virus were tagged with the enhanced green fluorescent protein (eGFP; Fig. 1C', D'); neurons that were positive for both fluorescent reporters (mCherry+/eGFP+) were considered 'starter neurons' (Fig. 1E, F). Choline acetyltransferase (ChAT) immunolabeling was used to determine the cholinergic phenotype of starter neurons and locate the injection sites within the PPN/LDT rostro-caudal distribution (Fig. 1C'', D''). The cholinergic phenotype of the starter neurons was in some cases difficult to assess, as transduced neurons show immunohistochemical interference. The total average of starter neurons for the PPN was 98.33 ± 18.95 and 62 ± 7.58 for the LDT. Injections in the PPN were targeted to the rostral ($n=3$ rats) and caudal ($n=3$ rats) portions of the nucleus, injections in the LDT were targeted at its center ($n=3$ rats; Fig. 1B). Following initial analysis, the data obtained from both regions of the PPN (i.e. rostral and caudal) were pooled together ($n=6$ rats) given the similarity in the mapping of the areas projecting to each PPN region and the number of presynaptic neurons counted. The LDT group also showed consistent result across animals despite the reduced n , nevertheless the results should be interpreted with caution.

Monosynaptically-labeled eGFP input neurons were distributed in a wide range of brain regions including the cortex, basal ganglia, forebrain, thalamus, hypothalamus, midbrain and upper and lower brainstem. eGFP labeling was intensely distributed along the neurons' dendritic arbor and axonal projections (Fig. 1E'). Animals that had injections out of target, that had injections that overlapped between cholinergic nuclei, or where the quality of the labeling was poor (few input neurons or faint labeling), were not considered for further analysis. Control brains in which the helper viruses were omitted ($n=3$) did not display any type of presynaptic labeling, confirming the cell-type specificity for input tracing (not shown).

Inputs to cholinergic neurons arise from widespread functional areas. To determine whether afferents to the distinct domains that compose the cholinergic midbrain originate in overlapping or separate brain regions, input neurons were initially grouped according to large functional divisions, i.e. cortex, basal ganglia, forebrain, thalamus, hypothalamus, midbrain and brainstem (Fig. 2A) in male and female animals. We found that the midbrain and brainstem regions provide the largest number of input neurons to both PPN and LDT; both structures receive significantly more afferents from these functional areas than from the forebrain and the thalamus (two-way ANOVA; interaction: $F(6,49) = 0.918$; $P = 0.490$; PPN main effects: $F(6,48) = 11.713$; $P < 0.001$; Bonferroni corrected pairwise comparisons: midbrain vs forebrain/thalamus $P < 0.001$, brainstem vs forebrain/thalamus $P = 0.001$; LDT main effects: $F(6,48) = 5.239$; $P < 0.001$; Bonferroni corrected pairwise comparisons: midbrain vs forebrain $P = 0.011$; midbrain vs thalamus $P = 0.005$, brainstem vs forebrain $P = 0.002$, brainstem vs thalamus $P = 0.005$). In the PPN, only the basal ganglia showed a comparable number of input neurons to the midbrain/brainstem after rabies tracing (basal ganglia vs midbrain $P = 0.904$; basal ganglia vs brainstem $P = 0.535$). In contrast, the LDT receives a larger number of cortical inputs compared to the PPN (see below). The distribution of data shows that the individual values of males and females overlap, so it is unlikely that there exist sexual anatomical differences. Overall, while PPN and LDT share a similar distribution of input neurons across distinct brain regions (Fig. 2B), and this is particularly evident in the midbrain and brainstem, the most notable differences were observed in the basal ganglia (for PPN) and the cortex (for LDT).

Monosynaptic inputs from individual brain structures. To determine the differences in the innervation to PPN and LDT cholinergic neurons from individual structures among the above-defined functional regions, we examined the total number of neurons across all of those brain structures that fulfilled the criteria

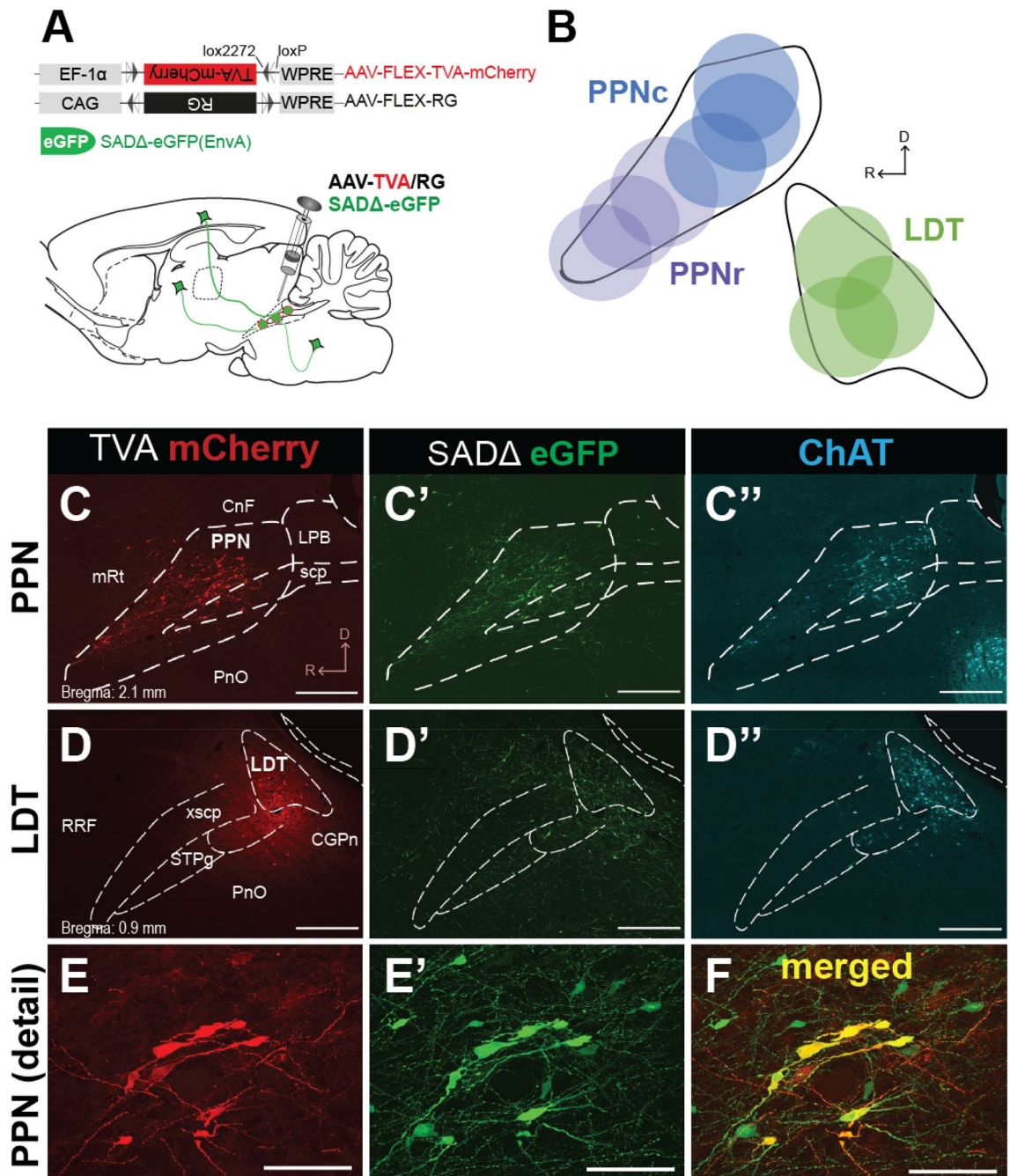


Figure 1. Transsynaptic retrograde tracing of midbrain cholinergic neurons. (A) Schematic of the experimental procedure. AAV5-FLEX-TVA-mCherry and AAV8-FLEX-RG helper viruses were injected into the PPN or LDT of rats that expressed Cre in cholinergic neurons. Two weeks after these injections, a modified rabies virus SADΔG-eGFP (EnvA) was injected into the same area and the brain was processed after 7 days. (B) Location of the site of injections in the PPN and LDT. (C–E) Injections were confined to the borders of the PPN (C–C') and LDT (D–D'), as determined by ChAT immunolabeling in parasagittal sections (C'' and D''). E, Starter neurons were identified by the expression of the TVA helper reporter and SADΔ-eGFP. Scale bars (C) and (D): 1 mm. (E–F): 100 μm.

described in the Methods (total: 50 structures; Fig. 3). The average total number of input neurons was 1508 ± 428 for the PPN and 874 ± 115 for the LDT. Analysis of the proportional contribution of each structure relative to the overall total number of input neurons to the PPN and the LDT for each animal revealed that several structures in the midbrain and the basal ganglia preferentially innervate the PPN. We observed that the vast majority of inputs to PPN cholinergic neurons originated in SC ($10.24\% \pm 2.45$, 356 ± 86 average number of neurons). Within the SC, input neurons were preferentially located in the deep gray layer (DpG, $38.5\% \pm 4.6$) but neurons also distributed notably in the deep (DpWh, $23.12\% \pm 3.44$) and intermediate white layers (InWh, $18.82\% \pm 4.5$)

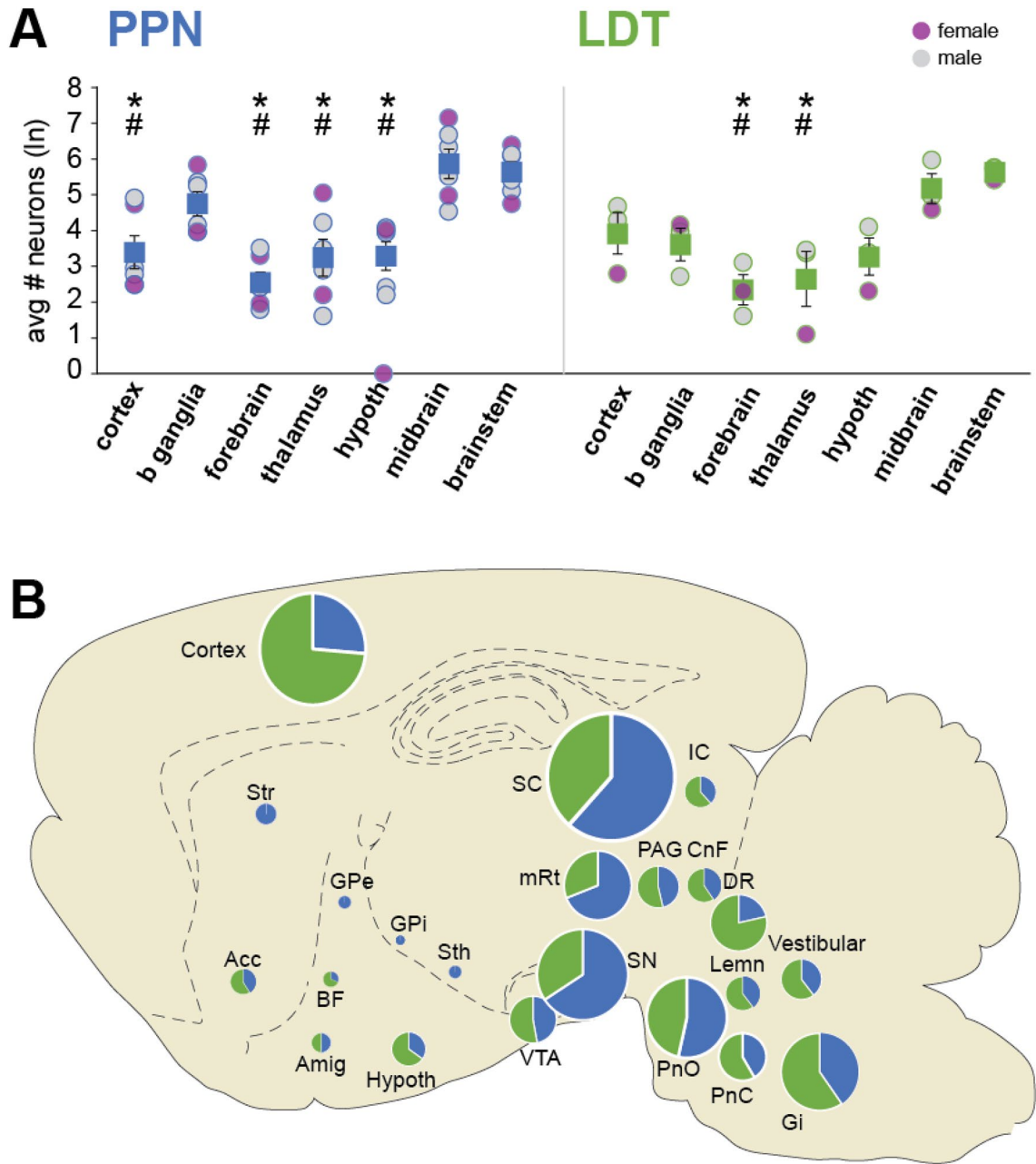


Figure 2. Afferents to PPN and LDT cholinergic neurons are heterogeneously distributed across brain regions. **(A)** Average number (natural logarithm [ln], mean \pm SEM) and individual subject values of input neurons (PPN $n = 6$ rats; LDT $n = 3$ rats) grouped by anatomical region, representing the cortex, basal ganglia, forebrain, thalamus, hypothalamus, midbrain and brainstem (see Fig. 3 for the list of structures that were grouped in each major region). Input neurons were more concentrated in the midbrain and brainstem for both PPN and LDT, and in the basal ganglia for the PPN. *, significant when compared to midbrain; #, significant when compared to brainstem. **(B)** Summary schematic illustrating the distribution of input neurons across the brain. The pie charts show the percentage of neurons projecting to the PPN or LDT, whereas the size of the chart shows the relative strength of this connection as estimated by the number of neurons. See list of abbreviations in Table 1.

as well as in the intermediate gray layer (InG, $16.86\% \pm 1.23$). The SC is equally an important input source for the LDT ($6.40\% \pm 1.49$, 98.66 ± 26.14 average number of neurons); no significant differences were detected between PPN and LDT. Within the SC, the majority of input neurons to the LDT were also localized preferentially in the DpG ($39.58\% \pm 5.54$). Other midbrain structures such as the interstitial nucleus of Cajal (int cajal), the brachium of the inferior colliculus (BIC), the red nucleus, the parabrachial, the mesencephalic reticular formation (mRT) and the precuneiform (PrCnf), were found to have significantly more input neurons innervating the PPN than the LDT (two-tailed t-tests, int cajal $P = 0.036$, BIC $P = 0.009$, red nucleus $P = 0.036$, parabrachial nucleus $P = 0.016$, mRT $P = 0.052$, PrCnf $P = 0.044$). After the SC, the second most important input region to the PPN was the SN ($7.39\% \pm 0.39$; 225 ± 36 neurons) which included neurons located in both, the pars compacta and pars reticulata.

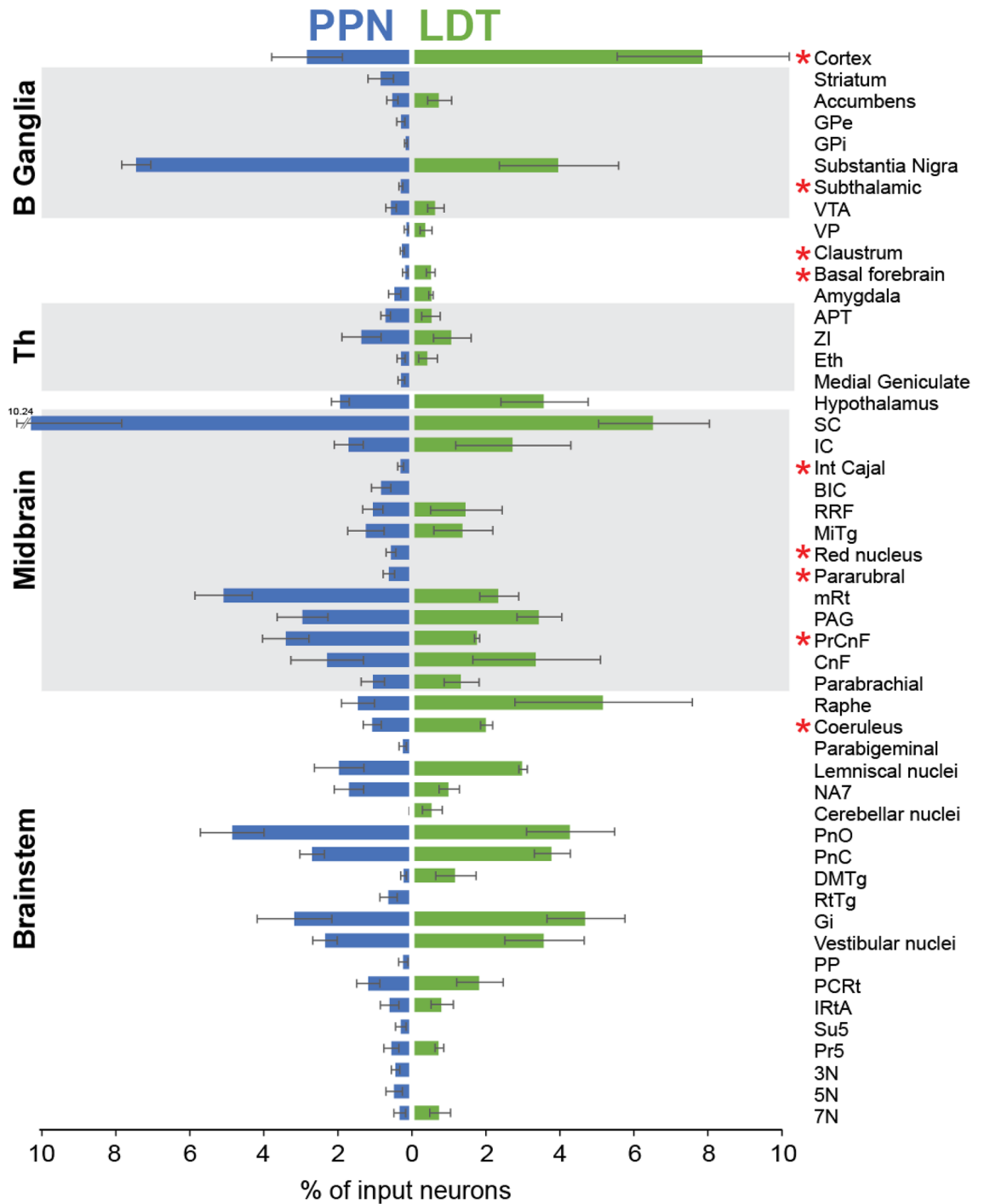


Figure 3. Major input structures to the cholinergic neurons of the PPN and LDT. Histogram showing the percentage of eGFP+ input (transsynaptically-labeled) neurons after injections of modified rabies virus in the PPN and LDT. The percentage is normalized by the total number of input neurons and the structures were organized in functional areas. Two-sided t tests were used to compare differences between the number of input neurons to the PPN and LDT from all structures (* $P \leq 0.05$). Mean \pm SEM (PPN $n = 6$ rats; LDT $n = 3$ rats). See list of abbreviations in Table 1.

Compared to the PPN-injected animals, LDT-injected animals showed half of the input neurons in the SN ($3.855\% \pm 1.6$; 62.66 ± 9.83 neurons), although the difference was not significant ($P = 0.07$). Similarly, the globus pallidus pars interna (GPe) and the subthalamic nucleus (STN) provide more input neurons to the PPN than the LDT (two-tailed t tests, GPe $P = 0.086$, STN $P = 0.01$). In contrast, the largest source of inputs to the LDT was the cerebral cortex ($7.73\% \pm 2.31$; 122 ± 24.9 neurons) and this is in stark contrast to the PPN (2.76 ± 0.95 ; 99.33 ± 22 neurons; two-tailed t test $P = 0.047$). Another important input region to the LDT was the raphe ($5.05\% \pm 2.38$, 86 ± 34 neurons), which included the dorsal raphe (DR), with its ventral and dorsal segments, and the median

and paramedian raphe nuclei. In addition, the locus coeruleus contained more input neurons for the LDT than for the PPN (two-tailed *t* test $P=0.044$, 33.3 ± 4 neurons vs 20 ± 12.4 neurons); the remaining brainstem structures examined did not show any preference for PPN or LDT. These results support a differential afferent balance between PPN and LDT according to the functional circuits in which they are embedded, where PPN cholinergic neurons preferentially receive inputs from structures involved in motor functions, whereas LDT cholinergic neurons receive a larger number of inputs from LC, DR and structures involved in limbic functions.

Cortical inputs to the cholinergic midbrain. To further characterize the differences in the afferents from the cerebral cortex to the cholinergic midbrain, we identified the different cortical regions where input neurons were present, revealing different patterns between PPN and LDT. Cortical input neurons were distributed along the mediolateral axis and localized in the motor cortex (Fig. 4A) and somatosensory areas (SS), the orbitofrontal cortex (OFC) and anterior cingulate cortex (ACC; Fig. 4B). Input neurons in the motor cortex were similarly distributed between M1 and M2 areas, and because there were no differences in the number of input neurons between them, the data was pooled and presented as M1/M2 (MC, motor cortex). We observed that various primary somatosensory cortical areas project to the cholinergic midbrain; these neurons were located in the barrel cortex, the frontal lobe, and cortices that receive sensory inputs from the upper lip, jaw, trunk, shoulder and limbs. Input neurons within the OFC were distributed in the medial orbital area, orbital area, ventral orbital area, ventrolateral orbital area and agranular insular areas dorsal and ventral segments, and input neurons in ACC were mainly located in areas A24a, A24b, A25 and A32. The quantification of input neurons across these cortical areas revealed that PPN receives more inputs from MC ($1.41\% \pm 0.26$, 21.83 ± 8.97 neurons) than from other cortical regions (Kruskal–Wallis H test: $\chi^2(5)=13.456$, $P=0.019$; Bonferroni corrected post hoc tests: MC vs visual cortex: $P=0.015$; Fig. 4C). In contrast, the LDT receives most of its inputs from the OFC ($2.53\% \pm 1.93$, 22.33 ± 16.6 neurons), ACC ($2.04\% \pm 0.68$, 19.33 ± 8.09 neurons) and MC ($1.77\% \pm 0.42$, 16 ± 4.5 neurons; Kruskal–Wallis H test: $\chi^2(5)=13.141$, $P=0.022$; Fig. 4D). These results reveal that midbrain cholinergic neurons receive a specialized cortical input preferentially from either the MC, in the case of the PPN, or limbic cortices, in the case of the LDT.

Basal ganglia inputs to the cholinergic midbrain. To further characterize the differences in the afferents from the basal ganglia to the PPN and LDT, we compared the number of input neurons innervating each midbrain structure. The vast majority of inputs from basal ganglia structures to the PPN arises from the SN (SN, $7.39\% \pm 0.39$; 225 ± 36 neurons, Fig. 5A, E). Notably, we found input neurons in the striatum (Fig. 5B), which were identified as spiny projection neurons ($0.76\% \pm 0.34$; 12.66 ± 6.95 neurons Fig. 5B') with no specific distribution within striatal regions. Other basal ganglia inputs include the ventral striatum ($0.45\% \pm 0.15$, 8 ± 5.08 neurons), GPe ($0.21\% \pm 0.11$, 4.17 ± 2.21 neurons), GPi ($0.08\% \pm 0.03$, 2.66 ± 0.98 neurons), VTA ($0.48\% \pm 0.14$, 6.83 ± 3.2 neurons) and STN ($0.22\% \pm 0.05$, 3.5 ± 1.43 neurons). The number of inputs neurons in the SN, however, was significantly larger than in other basal ganglia structures (Kruskal–Wallis H test, $\chi^2(6)=17.379$, $P=0.008$; Bonferroni corrected post hoc tests: SN vs GPi: $P=0.009$; SN vs STN: $P=0.024$, SN vs GPe: $P=0.021$). LDT cholinergic neurons also received basal ganglia inputs, although this innervation was more restricted compared to that observed for the PPN. While the SN (62.66 ± 9.83 neurons) also provided the largest input to the LDT (Kruskal–Wallis H test, $\chi^2(6)=14.719$, $P=0.023$; Bonferroni corrected post hoc tests: SN vs STN: $P=0.043$; SN vs GPe: $P=0.043$), the rest of the basal ganglia inputs were distributed in ventral structures, such as the ventral striatum (0.64 ± 0.32 ; 5.66 ± 2.96 neurons Fig. 5C) and the VTA (0.54 ± 0.22 ; 4.66 ± 1.85 neurons Fig. 5D). No inputs to the LDT were observed to arise in the dorsal striatum or the STN. These results suggest that basal ganglia inputs to the cholinergic midbrain are functionally segregated, where dorsal basal ganglia structures innervate PPN cholinergic neurons, whereas ventral basal ganglia structures innervate LDT cholinergic neurons, in line with the functional segregation observed in cortical and midbrain areas. Notably, the SN seems to be a point of convergence of afferents to both cholinergic regions.

Immunohistochemical characterization of input neurons. Given that an important number of SN and DR neurons synapse onto PPN and LDT cholinergic neurons, we aimed to characterize them neurochemically on the basis of the immunohistochemical expression of tyrosine hydroxylase (TH) or tryptophan hydroxylase (TPH2), to identify dopaminergic and serotonergic neurons, respectively. In the SN, we found a large number of input neurons localized within the pars compacta and closely intermingled with TH+ neurons (Fig. 6A). However, in all cases input neurons were immunonegative for TH (Fig. 6A'). Similarly, in the DR, all input neurons were clearly identified within the borders set by the TPH2+ labeling (Fig. 6B), but none of the eGFP+ neurons were immunopositive for TPH2 (Fig. 6B'). We then reasoned that it is possible that the rabies-mediated GFP labeling interferes with the immunohistochemical detection on infected neurons (as we previously reported in Dautan et al., 2020). To test this possibility, we then incubated input neurons sections with an antibody against the ubiquitous neuronal marker NeuN, which produces widespread non-selective nuclear labeling in the brain, to determine whether this protein can be detected in rabies-infected input neurons. Similar to the immunodetection of TH and TPH, we were unable to identify immunopositive signal for NeuN among input neurons (Fig. 6C), suggesting that rabies labeling, the GFP protein or other unknown factors interfere with detection of neuronal markers when using immunohistochemistry. Given the anatomical distribution of input neurons in the SN and DR, however, it is likely that both dopaminergic and serotonergic neurons directly innervate cholinergic neurons of the PPN and the LDT.

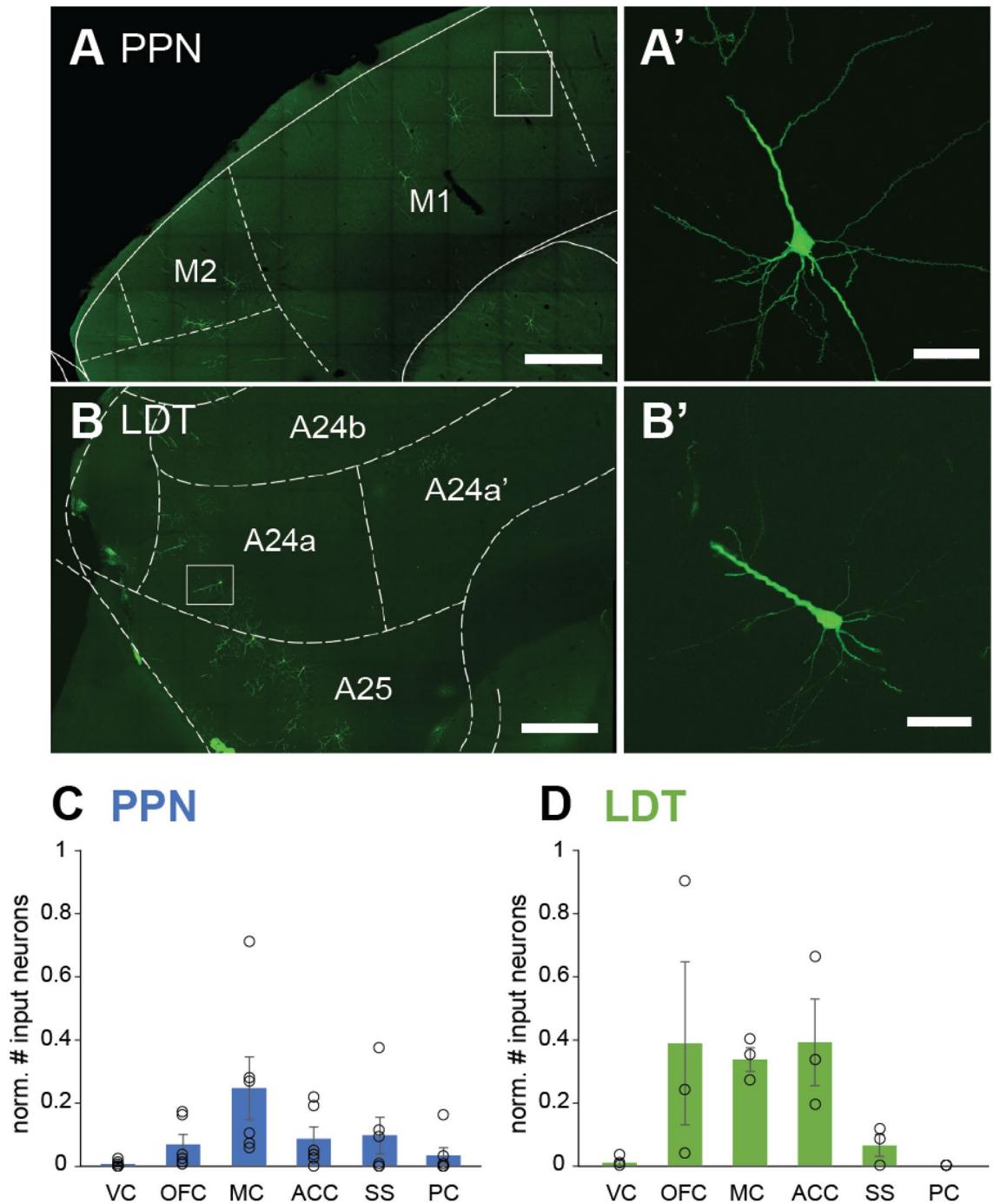


Figure 4. Distinct distribution of input neurons across cortical regions. **(A)** Fluorescent micrograph showing cortical input neurons to PPN cholinergic cells located in the motor cortex in a parasagittal section. **(A')** High magnification image of neuron in M1 (box in **A**). **(B)** Fluorescent micrograph showing input neurons to the LDT in the anterior cingulate cortex in a sagittal section. **(B')** High magnification image showing a neuron located in A24a (box in **B**). **(C)** Number of input neurons across cortical areas that innervate the cholinergic neurons of the PPN **(C)** and the LDT **(D)**, normalized to the number of starter neurons. VC, visual cortex; OFC, orbitofrontal cortex; MC, motor cortex (M1/M2); ACC, anterior cingulate cortex; SS, somatosensory cortex; PC, parietal cortex. Mean \pm SEM (PPN $n=6$ rats; LDT $n=3$ rats). Scale bars: **(A)** and **(B)**: 500 μm , **(A')** and **(B')**: 100 μm .

Discussion

In the present study we used a retrograde transsynaptic strategy to characterize the identity and whole-brain distribution of afferents that selectively innervate midbrain cholinergic neurons. We show that these afferents

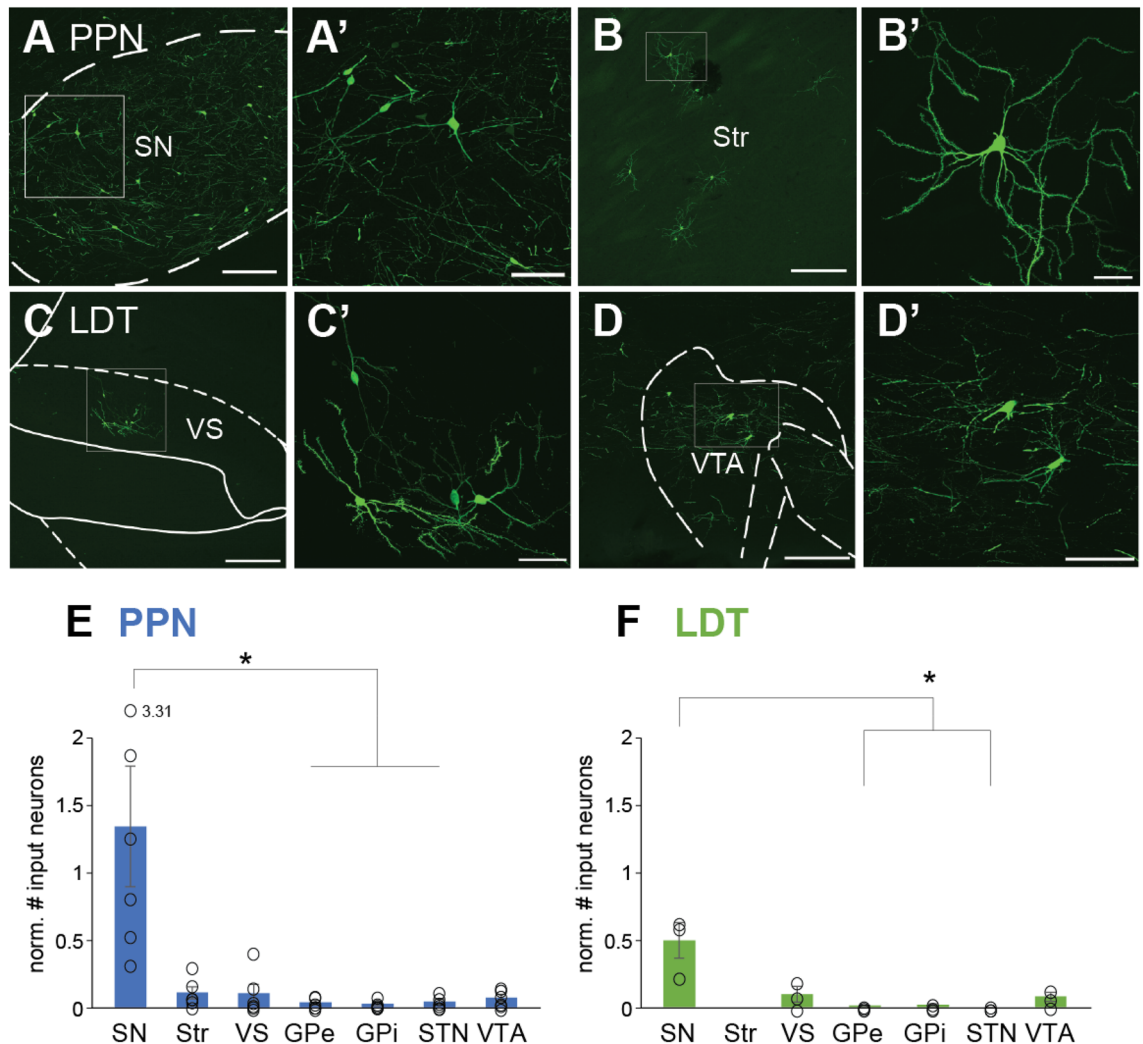


Figure 5. Basal ganglia input neurons predominantly target PPN. (A–D) Fluorescent micrographs in parasagittal sections showing basal ganglia input neurons that target the PPN (A, B) and LDT (C, D). Neurons located in the substantia nigra (SN) were predominantly observed after PPN injections (A–A′). Input neurons in the dorsal striatum were only observed following PPN injections (B–B′); note the presence of multiple spines in the dendritic arbor of the labeled neuron, suggesting that it is spiny projection neuron. In contrast, LDT injections produced labeling of input neurons in the ventral striatum (VS; C–C′) and the ventral tegmental area (VTA; D–D′). The normalized number of input neurons (to the number of starter neurons) reveal a differential distribution between the PPN (E) and LDT (F). For both cases, the majority of neurons localize in the SN. Mean \pm SEM (PPN $n=6$ rats; LDT $n=3$ rats). Kruskal–Wallis H test and Bonferroni corrected post hoc tests were performed to determine statistically significant differences, see text for values. Scale bars: (A), (B), (C) and (D), 250 μ m. (A′) and (D′) 100 μ m, (B′) and (C′) 50 μ m.

are widely distributed across the brain and reveal fundamental differences with other brain cholinergic systems (e.g. basal forebrain and striatal cholinergic interneurons; see below). Given the established differences in output connectivity and function between PPN and LDT, we hypothesized that segregated afferent systems selectively synapse on each midbrain cholinergic subset. Our data show that PPN and LDT share some of the most prominent inputs (i.e. SC and SN), but notably differ in the functional segregation between motor and limbic afferents innervating PPN and LDT, respectively. Our results suggest that the cholinergic neurons of the midbrain operate as a heterogeneous functional entity that is capable of processing incoming motor and limbic signals which are in turn conveyed through parallel specialized circuits, an idea that was first introduced for basal ganglia–thalamocortical loops²⁰, with which PPN/LDT maintain a close interconnectivity.

Afferent overlap vs input selectivity. Our data show that the SC constitutes the main input structure to both the cholinergic PPN and LDT, in line with initial studies describing the connectivity between these structures²¹. Input neurons in the SC were distributed in superficial, intermediate and deep layers, where there is a convergence of signals from visual, auditory and somatosensory modalities. Superficial layers receive input primarily from the retina and visual cortex. Deep layers, in contrast, receive inputs from several sensory modalities, inputs from motor areas, and projections from areas that are not purely sensory or motor²². It is likely that

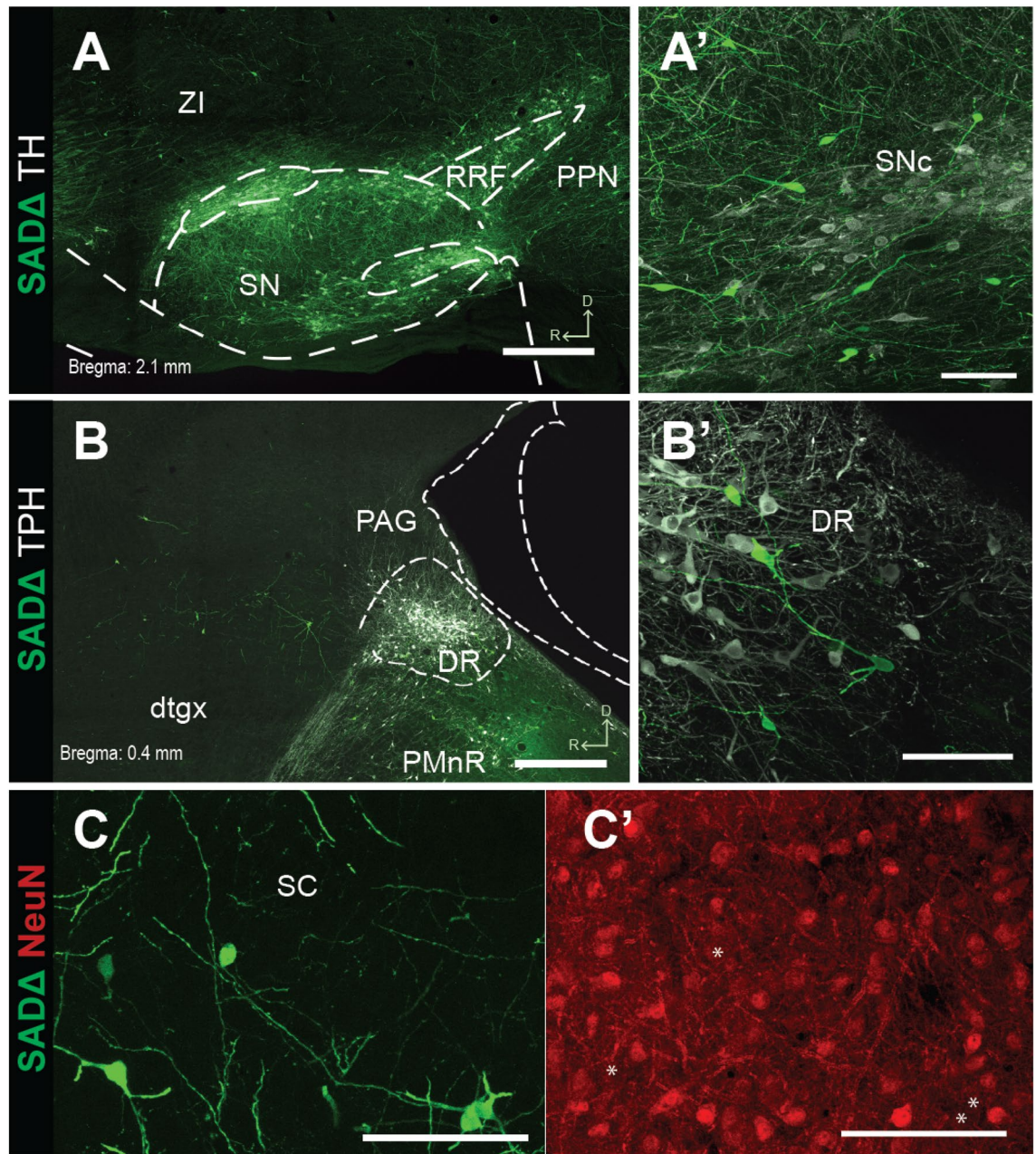


Figure 6. Neurochemical characterization of input neurons in the substantia nigra compacta and dorsal raphe. (A) Input neurons located within the borders of the SNc after injections in the PPN and LDT were immunolabeled with a TH antibody to identify dopaminergic neurons. In all cases, input neurons were immunonegative, despite being closely intermingled with TH+ neurons (A'). (B) Input neurons located within the borders of the DR after injections in the LDT were immunolabeled with a TPH antibody to identify serotonergic neurons. In all cases, input neurons were immunonegative, despite being closely intermingled with TPH2+ neurons (B'). (C) Input neurons located in the superior colliculus (SC) were incubated with NeuN antibodies to detect the presence of this ubiquitous neuronal protein. (C') SC input neurons were immunonegative for NeuN, thus confirming the limitations of immunohistochemical detection of neuronal markers in rabies-infected neurons. Scale bars: (A) and (B) 500 μ m; (A'), (B') and (C) 100 μ m.

such prominent input will transmit information about the orientation of the eyes, head and pinnae²³, but also likely to signal target selection, attention²⁴ and decision making²⁵.

In addition to the SC, we found that the SN also provides a prominent input to both the PPN and the LDT. It is well documented that the PPN maintains important reciprocal connectivity with most basal ganglia structures, but the position of the SN to modulate the LDT had not been established, although previous anatomical studies have shown projections from the SNc to the LDT²⁶. Nigral projections arising from the pars reticulata have been described in detail^{27,28} and are known to be the major input to the PPN. These synapses have been

electrophysiologically characterized *in vitro* and their stimulation induces inhibition of PPN neurons^{29,30}, which suggests that this projection is largely GABAergic in nature³¹. A similar role although less prominent could be underlying the connectivity between the pars reticulata and the LDT likely in the context of behavioral activation, as reported before⁹. Interestingly, we found a number of input neurons in the dorsal and ventral striatum from PPN- and LDT-injected animals, respectively. These striatal neurons were distinguished as spiny projection neurons, suggesting that midbrain cholinergic neurons form part of the striatal output, as also seen for PPN glutamatergic neurons^{11,32}. Further studies should determine the relevance of this projection and the striatal output system to which it belongs (i.e. direct vs indirect pathway). Our data thus support that the cholinergic midbrain is a crucial link for relaying signals from virtually all basal ganglia structures, possibly influencing thalamic circuits that transmit feed-forward information to basal ganglia and cortical circuits.

We reveal that the cortex provides an important number of input neurons to the cholinergic midbrain, particularly to the LDT. Cortical projections to the LDT have been reported using conventional neuronal tracers, predominantly originating from the medial prefrontal and orbital cortices^{21,26,33–35}. Our data show that input neurons in the OFC were found mainly in LDT-injected animals, but some were also present in the PPN group, thus likely providing a substrate for the involvement of the cholinergic midbrain in behavioral flexibility^{36–39}. Also notably, we found input neurons in the anterior cingulate cortex mainly in the LDT group, which supports an involvement of the LDT in reinforcement learning and reward-guided selection of actions^{40–43}. In contrast, we reveal a prominent input from MC (M1, M2) to the cholinergic PPN neurons. While the role of the cholinergic PPN in motor behavior is still elusive (see [Introduction](#); also discussed in Gut and Mena-Segovia et al., 2019)⁴⁴, a projection from the MC may reveal a role for PPN cholinergic neurons in movement preparation or a readiness-to-respond signal. Interestingly, however, the PPN has efferent connectivity with motor regions of the lower brainstem, such as the pontine nucleus part oral (PnO) and caudal (PnC), gigantocellular nucleus (Gi) and spinal trigeminal nuclei, as well as projections to the spinal cord^{45–49}. This suggests that motor commands generated in cortical motor areas are transmitted to PPN cholinergic neurons and related to brainstem motor regions. Notably, we found a large number of input neurons in motor nuclei of the brainstem reticular formation, including the Gi, PnO, PnC and raphe magnus, suggesting a bidirectional role in the transmission of motor signals. Interestingly, neurons in this region of the brainstem are associated with muscle atonia during REM sleep and given the role of PPN/LDT cholinergic neurons in REM sleep, it is possible that such connectivity bidirectionally modulates some aspects of the muscle tone across sleep cycles. Further experiments to fully elucidate the role of PPN cholinergic neurons in motor behavior are necessary. In contrast to the PPN, LDT cholinergic neurons receive more prominent inputs from the DR and the LC, presumably from serotonergic and noradrenergic neurons (although we were unable to identify markers for the former; see Fig. 6). These inputs support a role in the regulation of the level of brain activation during waking and sleep.

Input/output relationship of the cholinergic midbrain. Using conditional anterograde tracing of cholinergic neurons in ChAT::Cre rats, we have recently revealed the pattern of axonal innervation of PPN and LDT cholinergic neurons^{3,7,8}. These previous studies together with our current dataset allow us to correlate the connectivity maps of midbrain cholinergic neurons. PPN cholinergic neurons maintain reciprocal connections with the basal ganglia, in particular the SN, GPe and striatum, the SC and motor nuclei of the brainstem, such as PnO, PnC and Gi. Interestingly, the connectivity with the cortex is also reciprocal, particularly with the motor and anterior cingulate cortices. In contrast, largely unidirectional efferent connectivity was observed with most thalamic nuclei, the ventral pallidum and amygdala. LDT cholinergic neurons maintain reciprocal connections with the inferior colliculus, DR, Gi, SN and ventral striatum. No LDT cholinergic axons were detected in the cortex, suggesting that this pathway is unidirectional. Similar to the PPN, we also found unidirectional efferent connectivity with the thalamus, the ventral pallidum and amygdala, but also with the globus pallidus, the olfactory tubercle and the medial and lateral septa. This comparative analysis based on our previously published results suggests that PPN and LDT maintain different levels of interconnectivity with the basal ganglia, the cortex and brainstem motor nuclei, whereas notably the thalamus stands out as a virtually exclusive output structure.

Input specialization across brain cholinergic systems. Cholinergic neurons are distributed across the brain in anatomically defined cell clusters⁵⁰. Among them, cholinergic neurons of the basal forebrain and CINs share important functional properties with the cholinergic neurons of the PPN and LDT. For example, cholinergic neurons of the basal forebrain and the PPN/LDT increase their discharge during behavioral arousal⁵¹. Moreover, CINs and cholinergic PPN/LDT neurons were found to be critical for the modulation of striatal output neurons during action selection¹³. These studies raise the question of whether cholinergic signaling from these systems is functionally overlapping. Recent studies have provided the identification of presynaptic inputs to the cholinergic basal forebrain^{14,15} and CINs^{16,17}. The comparison of the distribution of input neurons in these studies with the one reported here reveals that PPN/LDT cholinergic inputs are far more widely distributed across different brain regions than the inputs to any of these two other cholinergic groups. Basal forebrain neurons receive inputs predominantly from dorsal and ventral striatum, and from some cortical regions (orbital and insular) and the central nucleus of the amygdala. CINs receive inputs from several cortical regions, including M1, M2, S1, V1 and CC. Notably, CINs receive a prominent input from the thalamus and GPe. Thus, PPN/LDT cholinergic neurons share striatal inputs with the basal forebrain and cortical inputs with the CINs, although the proportions seem to differ greatly. This suggests that, despite the functional overlap across these cholinergic systems, they are largely segregated in their inputs. On the other hand, the convergence from some of these afferent regions (i.e. striatum and cortex) on distinct subsets of cholinergic neurons suggests the existence of an underlying mechanism capable of integrating cholinergic signaling across distant brain areas.

Materials and methods

Animals. All experimental procedures were performed on adult male (PPN: $n=4$, LDT: $n=2$) and female ChAT::Cre + rats (PPN: $n=2$, LDT: $n=1$)⁵². Rats were maintained on a 12 h light/dark cycle (light on 7:00 A.M.) and ad libitum access to water and food. All procedures were performed in accordance with the Society for Neuroscience policy on the use of animals in neuroscience and the ARRIVE guidelines, and were approved by the Institutional Animal Care and Use Committee of Rutgers University, in compliance with the National Institutes of Health Guide for the Care and Use of Laboratory Animals.

Stereotaxic injections. Surgeries were performed under deep isoflurane anesthesia (2% in O₂; Isoflo; Schering-Plough). To demonstrate monosynaptic inputs to the PPN and LDT we used a transsynaptic tracing system based on the modified rabies virus strategy^{53,54}. For this, animals were injected with 500 nL of a 1:1 mixture containing rAAV5/EF1a-Flex-TVA-mCherry, titer 4.3e12 VP/mL, and rAAV5/CA-Flex-RG, titer 2e12 VP/mL (both from University of North Carolina vector core). Injections targeted the rostral (500 nL over 10 min; from bregma in mm: AP, -7.3; ML, +1.8; DV, -6.8 ventral of the dura; $n=3$) and caudal parts of the PPN (500 nL over 10 min; from bregma in mm: AP, -7.8; ML, +1.8; DV, -6.5 ventral of the dura; $n=3$). However, the results in terms of the distribution of input neurons did not show major differences between these two regions of the PPN and for this reason the data were pooled. Injections were also made in the LDT (500 nL over 10 min; from bregma in mm: AP, -8.5; ML, +0.9; DV, -6.0 ventral of the dura; $n=3$)⁵⁵. All injections were made using designated 1- μ l Hamilton syringes at a rate of 50 nL/min and post-injection diffusion time of 5 min. Fourteen days later, 500 nL of EnvA- Δ G-rabies-eGFP (Salk vector core, titer 4.3e8 transducing units [TU/mL])⁵⁴ were injected into the PPN and LDT using the same coordinates, the same rate of injection and diffusion time. Control experiments were performed where the modified rabies was injected to ChAT::Cre rats that did not receive any helper viruses.

Immunohistochemistry and imaging. Seven days after rabies virus injections, the rats were transcardially perfused with 0.05 M PBS, pH 7.4, followed by 300 ml of 4% w/v paraformaldehyde in phosphate buffer (0.1 M, pH 7.4). Brains were stored in phosphate buffer saline (PBS) with 0.05% azide at 4 °C until sectioning. Sagittal sections of 50 μ m thickness were obtained and collected in PBS, using a vibratome (VT1000S; Leica) and organized in series. We selected for our analysis one of every fourth section. For each brain, the site of injection was verified and only those with on-target injections were processed further. All the incubations were done in "Triton-PBS" (PBS containing 0.3% v/v Triton X-100 [Sigma]). Every fourth section was blocked for 2 h at room temperature (RT) while shaking in Triton-PBS containing 10% v/v of normal donkey serum (NDS; Jackson Immunoresearch). Next, they were incubated overnight in an anti-GFP antibody coupled with a 488 fluorophore (1:1000, Invitrogen, A-21311). Sections containing the sites of injection were incubated in rat-raised anti-GFP (1:1000, Nacalai tesque, 04404-84), rabbit anti-mCherry (1:1000, Abcam, ab167453) and goat anti-ChAT (1:500, Millipore AB 144P) overnight at RT. After washing, the sections were incubated for 4–6 h in the following secondary antibodies: donkey anti-rat 488 (1:500; Jackson Immunoresearch, 712-546-153), donkey anti-rabbit-Cy3 (1:500; Jackson Immunoresearch, 711-165-152) and donkey anti-goat 405 (1:500; Jackson Immunoresearch, 711-475-152) in Triton-PBS containing 1% of NDS. ChAT immunostaining was performed to delineate the borders of the PPN and LDT and assess the accuracy of our injections.

To determine the location and neurochemical identity of input neurons localized within the SN and dorsal raphe (DR), selected sections were incubated using antibodies against mouse tyrosine hydroxylase (TH) (1:1000, Sigma, T2928) and rabbit tryptophan hydroxylase 2 (1:500, Novus Biological, NB100-7455), respectively. Sections were then incubated in either donkey anti-mouse 405 (1:500; Jackson Immunoresearch, 715-475-151) or donkey anti-rabbit 405 (1:500; Jackson Immunoresearch, 711-475-152). To determine the expression of the neuronal marker NeuN in selected input neurons we used a mouse anti-NeuN antibody (1:500, Millipore Sigma, MAB 377) and a donkey anti-mouse 405 (same as above). After several washes, the fluorescently labeled sections were mounted on glass slides using Vectashield and examined on a confocal (FV-2000; Olympus) microscope. Whole-brain images were obtained by tiling (i.e. combining) and stitching (i.e. joining) individual images taken at 10 \times magnification. Sections were scanned at 10, 20 and 30 μ m in depth, thus generating three images per brain section.

Analysis of input neurons. The brightness and contrast of the captured images were adjusted in Photoshop (Adobe Systems) and superimposed with templates modified from an atlas to perform the mapping in the distinct brain areas⁵⁵. To quantify input cell numbers, we manually counted eGFP-positive neurons found on each of the three depths of the captured images per whole-brain section. We only recorded a positive neuron when we were able to identify its cell body in its entirety. Sections where only dendritic processes and axons or fractions of cell bodies were identified, were not counted. Thus, it is likely that our counting underestimated the total number of input neurons. We counted and registered in an excel spreadsheet the number and location of every input neuron found in each brain region throughout the most lateral to most medial levels using the counter cell in-built function of the ImageJ software. This was done for all brains included in this study ($n=9$). Brains with less than a total of 500 input neurons, which occurred when the transduction of starter neurons was limited, were not considered for analysis. From all the brain nuclei where we found input neurons within the PPN and LDT groups, we selected only those regions in which at least one of 3 animals had more than 5 neurons and the other two animals had more than 1 neuron. If one of the animals did not have any neuron in a given structure, that structure was not included in our final analysis. By applying these criteria, we obtained a list of 50 structures which are reported in this study (see Table 1 for abbreviations). Cells were counted by two experimenters, one of which remained blind for the entire phase of analysis.

3 N	Oculomotor n	NA7	Nucleus adrenergic 7
5 N	Motor trigeminal n	OFC	Orbitofrontal cortex
7 N	Facial n	PAG	Periaqueductal gray
ACC	Anterior cingular cortex	PC	Parietal cortex
APT	Anterior Pretectal nucleus	PCRt	Parvicellular reticular n
BIC	Brachium of superior colliculus	PMnR	Paramedian raphe nucleus
CnF	Cuneiform n	PnC	Pontine reticular n., caudal
DMTg	Dorsomedial tegmental area	PnO	pontine reticular n., oral
DpG	Deep gray layer SC	PP	peripeduncular n
DpWh	Deep white layer SC	PPN	Pedunculopontine n
DR	Dorsal raphe	Pr5	Principia sen. trigeminal n
dtgx	Dorsal tegmental decussation	PrCnF	Precuneiform area
Eth	Ethmoid thalamic n	RRF	Retrorubral Field
Gi	Gigantocellular reticular n	RtTg	Reticulotegmental n
GPe	Globus Pallidus pars externa	SC	Superior Colliculus
GPI	Globus Pallidus pars interna	SN	Substantia Nigra
IC	Inferior Colliculus	SNc	SN pars compacta
Int Cajal	Interstitial nucleus of Cajal	SS	Somatosensory cortex
InG	Intermediate gray layer SC	STN	Subthalamic n
InWh	Intermediate white layer SC	Su5	Supratrigeminal n
IRTA	Intermediate reticular n., alpha	VC	Visual cortex
LDT	Laterodorsal n	VP	Ventral Pallidum
MiTg	Microcellular tegmental n	VS	Ventral striatum
MC	Motor cortex	VTA	Ventral Tegmental Area
mRt	Mesencephalic reticular form	ZI	Zona Incerta

Table 1. List of abbreviations.

Experimental design and statistical analyses. For the comparison of the distribution of input neurons to PPN and the LDT we compared two experimental groups, rats injected in the PPN for the examination of input neurons to the PPN and rats injected in the LDT for the examination of input neurons to the LDT. For the evaluation of differences between the distribution of input neurons from different functional areas we considered two independent variables (target areas and functional input areas) and conducted 2-way ANOVAs on natural logarithm (ln)-transformed (to address the violation of the homogeneity of variances) numbers of input neurons followed by univariate tests to understand the simple main effects of the target structure on each functional area. To examine if selected structures within functional areas have more input neurons projecting to the PPN or LDT, respectively, than other structures, we used the Kruskal–Wallis H test, because the variances of the individual groups were heterogeneous. The counts of inputs neurons were normalized to either the total number of input neurons (Fig. 3) or the number of starter neurons (Figs. 4, 5). Post-hoc tests were Bonferroni-corrected. To compare differences between the number of input neurons to the PPN and LDT from all the individual structures that we identified to have input neurons, we conducted two-sided t-tests.

Received: 14 January 2021; Accepted: 30 March 2021

Published online: 27 April 2021

References

1. Steriade, M., Paré, D., Parent, A. & Smith, Y. Projections of cholinergic and non-cholinergic neurons of the brainstem core to relay and associational thalamic nuclei in the cat and macaque monkey. *Neuroscience* **25**, 47–67 (1988).
2. Parent, M. & Descarries, L. Acetylcholine innervation of the adult rat thalamus: distribution and ultrastructural features in dorso-lateral geniculate, parafascicular, and reticular thalamic nuclei. *J. Comp. Neurol.* **511**, 678–691 (2008).
3. Huerta-Ocampo, I., Hacıoğlu-Bay, H., Dautan, D. & Mena-Segovia, J. Distribution of midbrain cholinergic axons in the thalamus. *eNeuro* <https://doi.org/10.1523/ENEURO.0454-19.2019> (2020).
4. Woolf, N. J. & Butcher, L. L. Cholinergic systems in the rat brain: III. Projections from the pontomesencephalic tegmentum to the thalamus, tectum, basal ganglia, and basal forebrain. *Brain Res. Bull.* **16**, 603–637 (1986).
5. Clarke, P. B. S., Hommer, D. W., Pert, A. & Skirboll, L. R. Innervation of substantia nigra neurons by cholinergic afferents from pedunculopontine nucleus in the rat: neuroanatomical and electrophysiological evidence. *Neuroscience* **23**, 1011–1019 (1987).
6. Bolam, J. P., Francis, C. M. & Henderson, Z. Cholinergic input to dopaminergic neurons in the substantia nigra: a double immunocytochemical study. *Neuroscience* **41**, 483–494 (1991).
7. Dautan, D. *et al.* A major external source of cholinergic innervation of the striatum and nucleus accumbens originates in the brainstem. *J. Neurosci.* **34**, 4509–4518 (2014).
8. Dautan, D., Hacıoğlu Bay, H., Bolam, J. P., Gerdjikov, T. V. & Mena-Segovia, J. Extrinsic sources of cholinergic innervation of the striatal complex: a whole-brain mapping analysis. *Front. Neuroanat.* **10**, 1 (2016).
9. Dautan, D. *et al.* Segregated cholinergic transmission modulates dopamine neurons integrated in distinct functional circuits. *Nat. Neurosci.* **19**, 1025–1033 (2016).

10. Xiao, C. *et al.* Cholinergic mesopontine signals govern locomotion and reward through dissociable midbrain pathways. *Neuron* **90**, 333–347 (2016).
11. Roseberry, T. K. *et al.* Cell-type-specific control of brainstem locomotor circuits by basal ganglia. *Cell* **164**, 526–537 (2016).
12. Kroeger, D. *et al.* Cholinergic, glutamatergic, and GABAergic neurons of the pedunculopontine tegmental nucleus have distinct effects on sleep/wake behavior in mice. *J. Neurosci.* **37**, 1352–1366 (2017).
13. Dautan, D. *et al.* Cholinergic midbrain afferents modulate striatal circuits and shape encoding of action strategies. *Nat. Commun.* <https://doi.org/10.1038/s41467-020-15514-3> (2020).
14. Do, J. P. *et al.* Cell type-specific long-range connections of basal forebrain circuit. *Elife* <https://doi.org/10.7554/eLife.13214> (2016).
15. Gielow, M. R. & Zaborszky, L. The input–output relationship of the cholinergic basal forebrain. *Cell Rep.* **18**, 1817–1830 (2017).
16. Klug, J. R. *et al.* Differential inputs to striatal cholinergic and parvalbumin interneurons imply functional distinctions. *Elife* <https://doi.org/10.7554/eLife.35657> (2018).
17. Guo, Q. *et al.* Whole-brain mapping of inputs to projection neurons and cholinergic interneurons in the dorsal striatum. *PLoS ONE* **10**, e0123381 (2015).
18. Mena-Segovia, J. Structural and functional considerations of the cholinergic brainstem. *J. Neural Transm.* **123**, 731–736 (2016).
19. Callaway, E. M. & Luo, L. Monosynaptic circuit tracing with glycoprotein-deleted rabies viruses. *J. Neurosci.* **35**, 8979–8985 (2015).
20. Alexander, G. E., Crutcher, M. D. & DeLong, M. R. Basal ganglia-thalamocortical circuits: parallel substrates for motor, oculomotor. *Prog. Brain Res.* **85**, 119–146 (1990).
21. Semba, K. & Fibiger, H. C. Afferent connections of the laterodorsal and the pedunculopontine tegmental nuclei in the rat: a retro- and antero-grade transport and immunohistochemical study. *J. Comp. Neurol.* **323**, 387–410 (1992).
22. Cang, J., Savier, E., Barchini, J. & Liu, X. Visual function, organization, and development of the mouse superior colliculus. *Annu. Rev. Vis. Sci.* **4**, 239–262 (2018).
23. Sparks, D. L. Translation of sensory signals into commands for control of saccadic eye movements: role of primate superior colliculus. *Physiol. Rev.* **66**, 118–171 (1986).
24. Krauzlis, R. J., Lovejoy, L. P. & Zénon, A. Superior colliculus and visual spatial attention. *Annu. Rev. Neurosci.* **36**, 165–182 (2013).
25. Wang, L., McAlonan, K., Goldstein, S., Gerfen, C. R. & Krauzlis, R. J. A causal role for mouse superior colliculus in visual perceptual decision-making. *J. Neurosci.* **40**, 3768–3782 (2020).
26. Cornwall, J., Cooper, J. D. & Phillipson, O. T. Afferent and efferent connections of the laterodorsal tegmental nucleus in the rat. *Brain Res. Bull.* **25**, 271–284 (1990).
27. Edley, S. M. & Graybiel, A. M. The afferent and efferent connections of the feline nucleus tegmenti pedunculopontinus, pars compacta. *J. Comp. Neurol.* **217**, 187–215 (1983).
28. Beckstead, R. M., Domesick, V. B. & Nauta, W. J. Efferent connections of the substantia nigra and ventral tegmental area in the rat. *Brain Res.* **175**, 191–217 (1979).
29. Noda, T. & Oka, H. Nigral inputs to the pedunculopontine region: intracellular analysis. *Brain Res.* **322**, 332–336 (1984).
30. Scarnati, E., Proia, A., Di Loreto, S. & Pacitti, C. The reciprocal electrophysiological influence between the nucleus tegmenti pedunculopontinus and the substantia nigra in normal and decorticated rats. *Brain Res.* **423**, 116–124 (1987).
31. Childs, J. A. & Gale, K. Neurochemical evidence for a nigrothalamic GABAergic projection. *Brain Res.* **258**, 109–114 (1983).
32. Caggiano, V. *et al.* Midbrain circuits that set locomotor speed and gait selection. *Nature* **553**, 455–460 (2018).
33. Satoh, K. & Fibiger, H. C. Cholinergic neurons of the laterodorsal tegmental nucleus: efferent and afferent connections. *J. Comp. Neurol.* **253**, 277–302 (1986).
34. Terreberry, R. R. & Neafsey, E. J. The rat medial frontal cortex projects directly to autonomic regions of the brainstem. *Brain Res. Bull.* **19**, 639–649 (1987).
35. Takagishi, M. & Chiba, T. Efferent projections of the infralimbic (area 25) region of the medial prefrontal cortex in the rat: an anterograde tracer PHA-L study. *Brain Res.* **566**, 26–39 (1991).
36. Amodeo, L. R., McMurray, M. S. & Roitman, J. D. Orbitofrontal cortex reflects changes in response-outcome contingencies during probabilistic reversal learning. *Neuroscience* **345**, 27–37 (2017).
37. Dalton, G. L., Wang, N. Y., Phillips, A. G. & Floresco, S. B. Multifaceted contributions by different regions of the orbitofrontal and medial prefrontal cortex to probabilistic reversal learning. *J. Neurosci.* **36**, 1996–2006 (2016).
38. Murray, E. A. & Rudebeck, P. H. Specializations for reward-guided decision-making in the primate ventral prefrontal cortex. *Nat. Rev. Neurosci.* **19**, 404–417 (2018).
39. Izquierdo, A. Functional heterogeneity within rat orbitofrontal cortex in reward learning and decision making. *J. Neurosci.* **37**, 10529–10540 (2017).
40. Schweimer, J. & Hauber, W. Involvement of the rat anterior cingulate cortex in control of instrumental responses guided by reward expectancy. *Learn. Mem.* **12**, 334–342 (2005).
41. Bohn, I., Gierler, C. & Hauber, W. Orbital prefrontal cortex and guidance of instrumental behaviour in rats under reversal conditions. *Behav. Brain Res.* **143**, 49–56 (2003).
42. Cardinal, R. N. *et al.* Role of the anterior cingulate cortex in the control over behavior by Pavlovian conditioned stimuli in rats. *Behav. Neurosci.* **117**, 566–587 (2003).
43. Hillman, K. L. & Bilkey, D. K. Neurons in the rat anterior cingulate cortex dynamically encode cost-benefit in a spatial decision-making task. *J. Neurosci.* **30**, 7705–7713 (2010).
44. Gut, N. K. & Mena-Segovia, J. Dichotomy between motor and cognitive functions of midbrain cholinergic neurons. *Neurobiol. Dis.* **128**, 59–66 (2019).
45. Martinez-Gonzalez, C., van Andel, J., Bolam, J. P. & Mena-Segovia, J. Divergent motor projections from the pedunculopontine nucleus are differentially regulated in Parkinsonism. *Brain Struct. Funct.* **219**, 1451–1462 (2014).
46. Grofova, I. & Keane, S. Descending brainstem projections of the pedunculopontine tegmental nucleus in the rat. *Anat. Embryol. (Berl)* **184**, 275–290 (1991).
47. Rye, D. B., Lee, H. J., Saper, C. B. & Wainer, B. H. Medullary and spinal efferents of the pedunculopontine tegmental nucleus and adjacent mesopontine tegmentum in the rat. *J. Comp. Neurol.* **269**, 315–341 (1988).
48. Chen, T.-W., Li, N., Daie, K. & Svoboda, K. A map of anticipatory activity in mouse motor cortex. *Neuron* **94**, 866–879.e4 (2017).
49. Spann, B. M. & Grofova, I. Origin of ascending and spinal pathways from the nucleus tegmenti pedunculopontinus in the rat. *J. Comp. Neurol.* **283**, 13–27 (1989).
50. Mesulam, M. M. Chapter 26 Human brain cholinergic pathways. *Prog. Brain Res.* **84**, 231–241 (1990).
51. Jones, B. E. Modulation of cortical activation and behavioral arousal by cholinergic and orexinergic systems. *Ann. N Y Acad. Sci.* **1129**, 26–34 (2008).
52. Witten, I. B. *et al.* Recombinase-driver rat lines: tools, techniques, and optogenetic application to dopamine-mediated reinforcement. *Neuron* **72**, 721–733 (2011).
53. Watabe-Uchida, M., Zhu, L., Ogawa, S. K., Vamanrao, A. & Uchida, N. Whole-brain mapping of direct inputs to midbrain dopamine neurons. *Neuron* **74**, 858–873 (2012).
54. Wickersham, I. R. *et al.* Monosynaptic restriction of transsynaptic tracing from single, genetically targeted neurons. *Neuron* **53**, 639–647 (2007).
55. Paxinos, G. & Watson, C. *The Rat Brain in Stereotaxic Coordinates* 6th edn. (Elsevier Academic Press, 2007).

Acknowledgements

We thank Yixin Tong and Selime Askit for their technical support in the acquisition of confocal images. This research was supported by NIH Grant NS100824 (J.M.S.), a NARSAD Young Investigator Award (J.M.S.) and Rutgers University.

Author contributions

I.H.O. and J.M.S. conceptualized the project and designed experiments. I.H.O., D.D. and B.K. conducted experiments. N.K.G. performed data analysis and helped editing the final version of the manuscript. I.H.O. and J.M.S. wrote the manuscript. All authors read and approved the final manuscript. J.M.S. supervised the project.

Competing interests

The authors declare no competing interests.

Additional information

Correspondence and requests for materials should be addressed to J.M.-S.

Reprints and permissions information is available at www.nature.com/reprints.

Publisher's note Springer Nature remains neutral with regard to jurisdictional claims in published maps and institutional affiliations.



Open Access This article is licensed under a Creative Commons Attribution 4.0 International License, which permits use, sharing, adaptation, distribution and reproduction in any medium or format, as long as you give appropriate credit to the original author(s) and the source, provide a link to the Creative Commons licence, and indicate if changes were made. The images or other third party material in this article are included in the article's Creative Commons licence, unless indicated otherwise in a credit line to the material. If material is not included in the article's Creative Commons licence and your intended use is not permitted by statutory regulation or exceeds the permitted use, you will need to obtain permission directly from the copyright holder. To view a copy of this licence, visit <http://creativecommons.org/licenses/by/4.0/>.

© The Author(s) 2021